ACADÉMIE
DES SCIENCES
INSTITUT DE FRANCE

Comptes Rendus
Chimie

Amina Abbaz, Sihem Arris and Abdeslam-Hassen Meniai

Equilibrium isotherm, kinetic, and thermodynamic studies of Safranin O adsorption on pomegranate (*Punica granatum*) peels as a low-cost adsorbent

Volume 28 (2025), p. 651-671

Online since: 12 September 2025

https://doi.org/10.5802/crchim.404

The Comptes Rendus. Chimie *are a member of the Mersenne Center for open scientific publishing*
www.centre-mersenne.org — e-ISSN : 1878-1543

ACADÉMIE DES SCIENCES
INSTITUT DE FRANCE

Comptes Rendus. Chimie
2025, Vol. 28, p. 651-671
https://doi.org/10.5802/crchim.404

Research article

Equilibrium isotherm, kinetic, and thermodynamic studies of Safranin O adsorption on pomegranate (*Punica granatum*) peels as a low-cost adsorbent

Amina Abbaz [a], Sihem Arris [a] and Abdeslam-Hassen Meniai [*, a]

[a] Environmental Process Engineering Laboratory (LIPE), Faculty of Process Engineering, University of Salah Boubnider Constantine 3, Constantine, 25000, Algeria

E-mail: meniai@yahoo.fr (A.-H. Meniai)

Abstract. The present study considered the adsorption capacity of Safranin O (SO) dye onto pomegranate peel powder (PP). The effect of operating parameters such as contact time, adsorbent dosage, initial concentration, pH and temperature on the performance of the dye adsorption process was also investigated. The PP was characterized by Fourier transform infrared spectroscopy (FTIR), X-ray diffraction (XRD), Thermogravimetric analysis (TGA), point of zero charge (pH_{pzc}), and Boehm titration. According to the results, the dye removal rate increased proportionally to the amount of adsorbent used. Langmuir, Freundlich, Temkin, and Dubinin–Radushkevich isotherms in their linear and non-linear forms were tested to determine the most appropriate model. The results showed an adsorption capacity by PP of 44 mg/g at natural pH, room temperature, in 30 min, and with an adsorbent dosage of 10 g/L. From the R^2, SSE, and RMSE values, it was found that the pseudo-second-order model best fitted the kinetic data and intraparticular diffusion was one of the rate-limiting steps. Thermodynamic analysis revealed that SO adsorption on PP is endothermic and favored. The results demonstrate that PP is a promising adsorbent for removing cationic dyes, such as SO, from aqueous solutions.

Keywords. Pomegranate, Adsorption, Kinetics, Safranin O, Dye, Wastewater.

Manuscript received 21 June 2024, revised 4 December 2024 and 26 March 2025, accepted 20 May 2025.

1. Introduction

Water is essential for sustainable and socio-economic development due to its impact on most aspects of economy and society. For instance, regardless of location, maintaining the quality of drinkable and safe water is crucial for public health [1,2]. The economy depends heavily on manufacturing processes, which also release residues and byproducts containing chemicals that, if improperly managed, could harm the environment and contaminate water sources [3]. In contrast to all other types of wastewaters, dye wastewater has drawn a great deal of attention. Over the past century, the printing and dyeing industries have released huge amounts of dyes into the environment [4]. Organic dyes are compounds widely used in various sectors as coloring agents in textiles, paper, rubber, leather, plastics, and other materials [5]. Nowadays, the textile industry uses over 700,000 tons of dyes and represents one of the three most significant sources of pollutants [6]. Most of the dyes used are organic compounds that are both carcinogenic and teratogenic [7]. Pharmaceutical and biochemical industries use Safranin O (SO), also known as basic red 2, as a dye in their histology and cytology sectors. It is commonly used

* Corresponding author

to identify cartilage, mucin, and mast cell granules as well as to stain gram-negative bacteria [8]. Moreover, it is frequently used in food products and for the coloration and processing of tannins, cotton, fibers, wool, paper, and leather [9].

Furthermore, SO may induce harmful health effects, including ocular irritation, dermatitis, and respiratory allergies. Considering these consequences, it is necessary to implement an appropriate wastewater treatment process [10]. Traditional remediating wastewater methods include sedimentation, coagulation, and chemical and membrane technologies. However, various drawbacks, including high costs, poor reusability, and low efficacy, frequently constrain these methods [11]. Therefore, two approaches have attracted much interest in the remediation of organic contaminants in wastewater. The first approach involves the degradation of organic pollutants using advanced oxidation processes. The degradation process produces highly reactive species. These species oxidize toxic organic compounds, breaking them into simpler, less harmful compounds, or entirely into CO_2 and water. The second approach is adsorption, which has emerged as a critical method for dye removal [12]. Adsorption is a flexible and inexpensive method to eliminate contaminants in wastewater. It is based on the contact of the adsorbate and a solid adsorbent for mass transfer [13]. Consequently, this approach has attracted interest in wastewater treatment because of its versatility and efficiency in handling a wide range of dyes. Adsorption processes have many advantages, including ease of use, performance in getting rid of dyes, and possibly even regeneration of the adsorbent for further use again [14,15]. This method is beneficial for treating wastewater persistently containing difficult-to-treat colors because it provides a suitable solution when other approaches are impractical.

Adsorbents, such as polymer resins, clay minerals, biomaterials, zeolites, carbon, and industrial solid waste, are used to remove organic pollutants from wastewater [13–15]. Adsorption is a simple and inexpensive process [16]. Activated carbon is the most commonly used adsorbent in this field because of its effectiveness in adsorption [17]. However, its application is limited because of its high cost and complex operation [18]. Adsorbents have several advantages over conventional chemical adsorbents in water treatment.

Even with the efficiency of these inexpensive adsorbents, their use has specific issues, like the difficulty of regeneration and treated water separation of treated water; these materials are affordable, biodegradable, readily available and manufactured. Adsorbents can be obtained from various biomasses, such as bacteria, fungi, algae, and industrial, natural, and agricultural waste [19–23]. These adsorbents are excellent at removing various contaminants from wastewater [24].

Among food and agricultural wastes, pomegranate (*Punica granatum*) peels (PPs) were considered to be highly effective in the removal of methylene blue [25], amaranth dye [26], hexavalent chromium [27], ciprofloxacin [28], and malachite green [29] from aqueous solutions. PP surface has functional groups like hydroxyl (–OH) and carboxyl (–COOH) that come from carboxylic acid, phenol, alcohol, ketone, aldehyde, ether, and ester parts. These groups are the main reason for its efficiency [30]. In 2020, the global area cultivated with pomegranates was approximately 300,000 hectares, producing about 3 million metric tons. The foremost pomegranate-producing countries include India, Turkey, the United States, China, Iran, Afghanistan, and Egypt. Since most of this quantity is turned into juice, jam, and other products, a significant amount of useless PP is generated [31].

Using PP as adsorbent for dye removal from aqueous solutions has gained significant interest due to their sustainability and cost-effectiveness. For instance, a study by Ahmed et al. found that PP was highly effective in removing dyes such as methylene blue [32].

This work investigates the removal of the SO dye using PPs, employing both linear and non-linear kinetic and isotherm models. Preparation and characterization of the PP adsorbent was the main focus of this work. Investigations were conducted into the effects of pH, initial concentration, temperature, and adsorbent mass. Equilibrium data were analyzed using isotherm parameters from the Langmuir, Freundlich, Temkin, and D–R linear and non-linear models. Different types of models were used to look into how to remove the SO dye from PPs. These included the pseudo-first-order, pseudo-second-order, Elovich, and intraparticle diffusion models. Additionally, thermodynamic parameters were analyzed to predict the adsorption process.

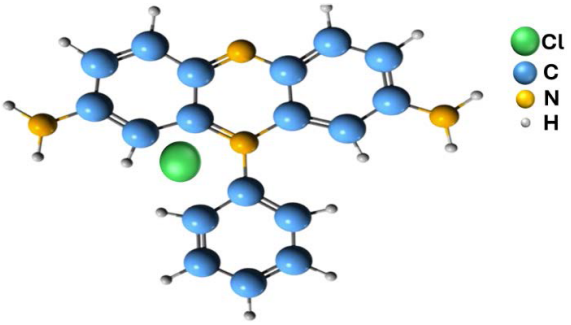

Figure 1. Chemical structure of Safranin O.

2. Materials and method

2.1. *Adsorbate and chemicals*

Analytical grade chemicals were used in the present work without any purification. Safranin O (λ_{max} = 522 nm, 99.5%), sodium hydroxide (99%), sodium chloride (99.5%), and hydrochloric acid (37%) were supplied by Sigma-Aldrich. The experiments reported in this paper used SO as the adsorbate, the chemical structure of which is shown in Figure 1.

2.2. *Adsorbent preparation*

Pomegranate peels were collected from a market in Mila, Algeria. Raw peels were washed with distilled water to remove any adhering substances, followed by drying in an oven at 50 °C for two hours. The dried PP was ground and sieved to achieve a uniform particle size of 315 µm and the resulting PP powder was then further oven-dried at 105 °C until a constant weight was obtained.

2.3. *Adsorbent characterization*

The surface functional groups of PP were studied using a Fourier transform infrared (FTIR) JASCO FT/IR 4600 spectrometer. The FTIR spectra of the powders were recorded at 4000 and 400 cm^{-1} frequencies.

The X-ray diffraction (XRD) measurements were performed using a D2 PHASER-BRUKER AXS diffractometer with Cu Kα radiation at a generator voltage of 40 kV and a generator current of 40 mA. The scattering angles (2θ) ranged from 5 to 100.

Thermogravimetric analysis (TGA) was conducted in an air atmosphere using a Mettler TC-10 apparatus, from 30 to 700 °C, at a heating rate of 10 °C/min.

The equilibrium pH of the adsorbent was measured by immersing 1 g of PP in 100 mL of distilled water. The whole was agitated for 24 h. After filtering the suspension, the pH of the filtrate was determined utilizing a pH meter.

The point of zero charge (pH_{pzc}) of PP was determined using the pH drift method [33]. Fifty mL of a 0.01 N NaCl solution was poured into six separate 250 mL Erlenmeyer flasks. Solutions 0.1 M NaOH and 0.1 M HCl were then used to adjust the pH between 2 and 12. Each flask was filled with 0.15 g of adsorbent and thoroughly shaken for 24 h. The pH in each flask was then determined. The pH_{zpc} value was then determined by plotting a graph of final pH vs. initial pH, and the intercept was selected as the pH_{pzc} of the PP surface.

The Boehm titration method was used to characterize functional groups as described by Farahani et al. [34]. A small amount (0.1 g) of PP adsorbent was mixed with 50 mL of solutions of 0.1 M NaOH, 0.1 M $NaHCO_2$, and 0.05 M Na_2CO_3, then shaken at room temperature for 96 h. Afterwards, the suspensions were decanted and filtered. The solutions were then back titrated with a 0.1 M HCl solution. An analogous procedure determined the basicity of the adsorbent. The sample was contacted with a 0.1 M HCl, and 0.1 M NaOH was used for the titration. The quantities of HCl and NaOH employed in titration are used to calculate surface chemistry. Acidic groups include lactones, phenolics, and carboxyls. The amount of 0.1 N HCl used to titrate the $NaHCO_2$ solution was used to figure out the carboxyl groups. Lactone groups were quantified by the difference in the consumed volume of 0.1 N HCl during the titration of Na_2CO_3 and $NaHCO_2$. Phenolic groups were identified by the difference in the consumed volume of HCl (0.1 N) during the titration of NaOH and Na_2CO_3 solutions. The volume of NaOH (0.1 N) required for the titration of HCl (0.1 N) was calculated to identify the basic groups. The quantity of functional groups can be calculated as follows:

$$\begin{aligned}\text{functional group (mmol/g)} &= \frac{(\text{Normality} \times \text{Volume}_{\text{Consumed}})}{\text{Adsorbent weight}} \\ &\times \frac{\text{(initial volume)}}{\text{(selected volume for titration)}}\end{aligned} \quad (1)$$

The iodine number, which quantifies the micropore content of an adsorbent (0–20 Å), was determined using a standard method [35]. In a conical flask, 10 mL of a 0.1 N iodine solution was titrated with a 0.1 N sodium thiosulfate solution. Two drops of a 1 wt% starch solution were employed as an indicator until the solution turned colorless. Fifty milligrams of PP were introduced into a conical flask containing 15 mL of a 0.1 N iodine solution, agitated for 4 min and then filtered. Ten milliliters of filtrate were titrated with a standard sodium thiosulfate solution, using two drops of starch solution as an indicator. The iodine number was calculated using the following equation:

$$\text{Iodine number} = \frac{(V_b - V_s) \times N \times (126.9) \times (15/10)}{M} \quad (2)$$

where V_b (mL) and V_s (mL) are the volumes of sodium thiosulfate solution required for blank and sample titrations, respectively, N (mol/L) is the normality of the sodium thiosulfate solution, 126.9 the atomic weight of iodine (g/mol), and M (g) the mass of PP used.

The methylene blue index (MBI) in mg/g indicates the adsorption capacity of medium-sized molecules for assessing mesopores and macropores. It is based on the method from the European Centre of Federations of the Chemical Industry (1989) [36]. In a 100 mL Erlenmeyer flask, 0.1 g of pre-dried PP and 50 mL of a 50 mg/L methylene blue solution were added. The mixture is agitated for 120 min and subsequently filtered. The residual concentration of methylene blue was measured using a UV–visible spectrophotometer at a wavelength of 665 nm. The methylene blue index was calculated according to the following equation:

$$\text{MBI} = \frac{(C_0 - C_r) \times V}{m} \quad (3)$$

where C_0 is the initial dye concentration (mg/L), C_r (mg/L) the residual dye concentration, V the solution volume (L) and m the mass of adsorbent (g).

The moisture content was determined by utilizing the oven-drying method. Half a gram of PP powder with an average particle size of 0.315 mm was placed in a weighed ceramic crucible. The samples were dried at 110 °C until they reached a stable weight. Subsequently, the samples were weighted after being cooled to room temperature [37]. The moisture content was calculated using the following formula:

$$\text{moisture (\%)} = \frac{w_3 - w_2}{w_1} \times 100 \quad (4)$$

where w_3 (g) is the weight of the crucible containing PP before drying, w_2 (g) is the weight of the crucible containing the PP after drying, and w_1 (g) is the weight of PP.

2.4. *Batch adsorption experiments*

Adsorption of SO on PP adsorbent was investigated by varying the dye concentration, pH, temperature, and adsorbent dose. The range of SO concentration was 10 to 300 mg/L. Using 0.1 N HCl and 0.1 N NaOH, the pH was adjusted from 2 to 12. The adsorbent dosage varied from 1 to 40 g/L. The experiment was carried out by changing the temperature from 298 to 333 K. Temperature variation is intended to determine thermodynamic parameters. The amount of dye adsorbed onto PP at time t q_t (mg/g) was assessed using an OPTIZEN POP UV–Vis spectrophotometer (K LAB Co., Ltd., Taejon, South Korea) at a wavelength of λ = 522 nm and calculated using the following equation:

$$q_t = \frac{(C_0 - C_t)}{m} \times V \quad (5)$$

Percentage removal (R%) was calculated by Equation (6):

$$R\% = \frac{(C_0 - C_t)}{C_0} \times 100 \quad (6)$$

where C_0 is the initial dye concentration (mg/L), C_t (mg/L) is the dye concentration at any time t, V is the volume of the solution (L), and m is the mass of adsorbent (g).

2.5. *Kinetic studies*

The kinetic studies of SO adsorption on PP were conducted using pseudo-first order, pseudo-second order, intraparticle diffusion, and Elovich models.

2.5.1. *Pseudo-first-order model*

According to Lagergren [38], the adsorption capacity of an adsorbent determines the solute's adsorption rate on it, which is represented by Equation (7).

$$\frac{dq_t}{dt} = k_1(q_e - q_t) \quad (7)$$

The linearized form of the pseudo-first-order model is expressed by:

$$\ln(q_e - q_t) = \ln q_e - k_1 t \tag{8}$$

where q_e and q_t are the amounts of adsorbed dye (mg/g) at equilibrium and at any time t (min), respectively, and k_1 (L·min^{-1}) is the pseudo-first-order model rate constant.

2.5.2. *Pseudo-second-order model*

The rate-limiting step in the pseudo-second-order model's one-step process is chemical adsorption, which creates valence forces by exchanging or sharing electrons between the adsorbent and the adsorbate [39]. Kinetic theory best describes the phenomenon using Equation (9).

$$\frac{\mathrm{d}q_t}{\mathrm{d}t} = k_2(q_e - q_t)^2 \tag{9}$$

The linearized form of the pseudo-second-order model equation is:

$$\frac{t}{q_t} = \frac{1}{k_2 q_e^2} + \frac{1}{q_e} t \tag{10}$$

where q_e and q_t (mg·g^{-1}) represent the amount of adsorbed dye at equilibrium and time t, respectively, the pseudo-second-order model's rate constant is denoted by k_2 (g·mg^{-1}·min^{-1}). The linearized relationship can be obtained by plotting t/q_t against t, with the intercept and the slope determining the values of k_2 and q_e, respectively.

2.5.3. *Intraparticle diffusion model*

The intraparticle diffusion kinetic model (Equation (11)) was used to investigate the rate-controlling step of SO adsorption [40].

$$q_t = k_\mathrm{i} t^{1/2} + C_\mathrm{i} \tag{11}$$

where k_i (mg·g^{-1}·min$^{1/2}$) is the intraparticle diffusion constant, and C_i is a constant depending on the boundary layer thickness. By plotting the linear determination between q_t and $t^{1/2}$, the values of k_i and C_i can be calculated by slope and intercept determination.

The following equation can be used to determine the intraparticle diffusion coefficient D_i, for SO adsorption onto PP:

$$D_\mathrm{i} = \frac{0.3r^2}{t_{1/2}} \tag{12}$$

where D_i is the coefficient of the intraparticle diffusion (cm^2·s^{-1}), $t_{1/2}$ is the time required to complete half the adsorption (s), and r is the radius of the adsorbent particle (cm). When the calculated value of D_i is located in the range of 10^{-5} to 10^{-13} cm^2·s^{-1}, it can be deduced that intraparticle diffusion is the rate-controlling step. In contrast, if it is between 10^{-6} and 10^{-8} cm^2·s^{-1}, the rate-controlling step is the film diffusion [41].

2.5.4. *Elovich model*

The type of chemisorption kinetics (homogeneous or heterogeneous) and the number of steps (one or multiple steps) contributing to the adsorption rate can be determined by applying the Elovich model to analyze adsorption rate data [42]. It can be expressed using Equation (13).

$$\frac{\mathrm{d}q_t}{\mathrm{d}t} = \alpha \exp^{-\beta q_t} \tag{13}$$

As $q_t \approx 0, \mathrm{d}q_t/\mathrm{d}t \approx \alpha$, integrating and applying the limits for t $(0, t)$ and q_t $(0, q_t)$, the Elovich model can be linearized as:

$$q_t = \frac{1}{\beta} \ln[1 + \alpha\beta t] \tag{14}$$

As the system approaches equilibrium $t \gg 1/\alpha\beta$, thus Equation (14) becomes:

$$q_t = \frac{1}{\beta} \ln(\alpha\beta) + \frac{1}{\beta} \ln t \tag{15}$$

where the desorption constant β (g·mg^{-1}) is related to surface coverage and the activation energy of chemical adsorption, α (mg·g^{-1}·min^{-1}) is the initial adsorption, and q_t (mg·g^{-1}) is the amount of dye adsorbed at time t (min). Plotting q_t versus $\ln t$ provides both α and β values.

2.6. *Isotherm adsorption experiment*

Adsorption isotherm experiments were established by equilibrating PP (0.5 g) in conical flasks holding 50 mL of dye solutions with various initial dye concentrations (50–300 mg·L^{-1}) at room temperature. The mixture was magnetically stirred at 150 rpm until achieving equilibrium. Samples were centrifuged once equilibrium was reached and analyzed for the residual SO concentrations. The amount of SO adsorbed by PP in each condition was calculated using Equation (5). The adsorption parameters were determined by using the following isotherm models:

2.6.1. *Langmuir isotherm model*

The most widely used adsorption isotherm is the Langmuir isotherm [43], which is based on three main assumptions: (i) monolayer adsorbate coverage is created on the homogeneous adsorbent surface; (ii) there is no interaction between the molecules that are retained; and (iii) the molecules of the adsorbate are connected to the adsorption active sites and are unable to migrate across the surface. The expression (16) represents the Langmuir equation.

$$q_e = \frac{q_m b C_e}{1 + bC_e} \tag{16}$$

The linearized form of Langmuir isotherm equation is:

$$\frac{1}{q_e} = \frac{1}{q_m} + \frac{1}{bq_m} \cdot \frac{1}{C_e} \tag{17}$$

where q_e is the amount of adsorbed SO at equilibrium (mg/g), C_e is the free SO concentration at equilibrium (mg/L), q_m is the maximum amount of adsorption for a complete monolayer (mg/g), and b is the constant associated with the binding site affinities and adsorption energy (L/mg).

The favorability of the process was assessed using the Langmuir isotherm's dimensionless constant separation factor (R_L). It is calculated using Equation (18). The isotherm's nature is indicated by R_L values, which can be either irreversible when $R_L = 0$, favorable when it is between 0 and 1, linear when $R_L = 1$, or unfavorable when it is higher than 1 [44].

$$R_L = \frac{1}{1 + bC_0} \tag{18}$$

where b is the constant of Langmuir, and C_0 is the initial SO concentration in the solution.

2.6.2. *Freundlich isotherm model*

The Freundlich isotherm is an empirical equation used to describe heterogeneous systems within a specific range. Furthermore, different adsorption energies occur in the active sites [45]. The Freundlich equation can be expressed as:

$$q_e = K_f C_e^{\frac{1}{n}} \tag{19}$$

The linearized form of Freundlich isotherm equation is as follows:

$$\ln q_e = \ln K_f + \frac{1}{n} \ln C_e \tag{20}$$

where q_e is the amount of adsorbed dye at equilibrium, K_f (mg·g^{-1}·(L·mg^{-1})$^{1/n}$) is the Freundlich constant corresponding to the capacity of adsorption; for a given adsorbate, an increase in K_f generally leads to a rise in adsorption capacity; $1/n$ is the Freundlich exponent associated with surface heterogeneity. Generally, if $1/n$ is between 0 and 1, it represents a favorable process; $1/n = 0$ indicates irreversible adsorption, and $1/n$ higher than 1 indicates unfavorable adsorption [46].

2.6.3. *Temkin isotherm model*

The Temkin isotherm considers the heat of adsorption over all molecules in the layer, which decreases linearly with coverage; this could be due to interactions between the adsorbate and adsorbent [47]. The Temkin isotherm can be represented as below.

$$q_e = \frac{RT}{b_T} \ln a_T C_e \tag{21}$$

The linearized form is described by the following equation:

$$q_e = B \ln a_T + B \ln C_e \tag{22}$$

where q_e is the amount of adsorbed dye at equilibrium, C_e (mg·L^{-1}) is the equilibrium concentration of SO at a constant temperature, q_e (mg·g^{-1}) is the amount adsorbed at equilibrium, a_T (L·g^{-1}) is the binding constant of the Temkin isotherm, and B (J·mol^{-1}) is the Temkin constant that is controlled by temperature. Calculating the intercept and slope of the plot q_e against $\ln C_e$ allows determining the values of B and a_T.

2.6.4. *Dubinin–Radushkevich (D–R)*

The D–R isotherm (Equation (23)) can be used to distinguish between chemisorption and physisorption. This isotherm explains the development of multilayers of microporous adsorbents; this is broader than the Langmuir isotherm because it does not require a homogeneous surface. However, it can be utilized to describe the adsorbent's surface heterogeneity at low coverage levels [48]. Equation (23) represents the D–R isotherm.

$$q_e = Q_m e^{-K_d \varepsilon^2} \tag{23}$$

The linear form of the D–R model is presented by the following equation:

$$\ln q_e = \ln Q_m - K_d \varepsilon^2 \tag{24}$$

where Q_m (mg·g^{-1}) is the adsorbed mass per unit weight of adsorbent at equilibrium, and

K_d ($mol^2 \cdot kJ^{-2}$) is the average adsorption energy per mole. The Polanyi potential ε can be calculated using Equation (25).

$$\varepsilon = RT \ln\left(1 + \frac{1}{C_e}\right) \tag{25}$$

where R (8.314 $J \cdot mol^{-1} \cdot K^{-1}$) and T (K) are the gas constant and the absolute temperature, respectively. The values of Q_m and K_d in Equation (13) can be acquired by obtaining the slope and intercept from a plot of $\ln q_e$ against ε^2. Equation (26) can be used to determine the mean free energy.

$$E = \frac{1}{\sqrt{2K_d}} \tag{26}$$

Chemisorption occurs when E is between 8 and 16 $kJ \cdot mol^{-1}$, while physisorption occurs when $E < 8$ $kJ \cdot mol^{-1}$ [49].

2.7. *Thermodynamic studies*

Thermodynamic studies provide information on the adsorption nature and feasibility by calculating the variations of relevant thermodynamic properties like enthalpy (ΔH) ($kJ \cdot mol^{-1}$), entropy (ΔS) ($J \cdot mol^{-1} \cdot K^{-1}$), and Gibbs free energy (ΔG) ($kJ \cdot mol^{-1}$) for dye absorption at various temperatures (20, 30, 40, 50, and 60 °C) using Equations (27)–(29) [50]:

$$\Delta G = -RT \ln K_d \tag{27}$$

$$\Delta G = \Delta H - T\Delta S \tag{28}$$

$$\ln K_d = \frac{\Delta S}{R} - \frac{\Delta H}{RT} \tag{29}$$

with R the universal gas constant (8.314 $J \cdot mol^{-1} \cdot K^{-1}$), K_d (q_e/C_e) the distribution coefficient and T (K) the absolute temperature. Plotting $\ln K_d$ versus $1/T$ leads to the determination of the thermodynamic parameters.

2.8. *Error functions*

A variety of mathematical error functions were used, including the following: coefficient of determination (R^2), the sum of squares errors (SSE), and root mean square error (RMSE). These functions were used to assess the reliability of linear and non-linear regression methods and to determine the best fit model for the experimental data [50,51].

$$\mathrm{SSE} = \sum_{i=1}^{n} (q_{e,\mathrm{exp}} - q_{e,\mathrm{cal}})_i^2 \tag{30}$$

$$\mathrm{RMSE} = \sqrt{\sum_{i=1}^{n} (q_{e,\mathrm{exp}} - q_{e,\mathrm{cal}})_i^2} \tag{31}$$

where $q_{e,\mathrm{cal}}$ is the computed value of the solid phase adsorbate concentration at equilibrium (mg/g) and $q_{e,\mathrm{exp}}$ is the experimental value. The number of data points is denoted by n.

3. Results and discussion

3.1. *Characterization analysis*

Figure 2a shows the FTIR spectrum of the SO dye and PP powder before and after SO adsorption. The spectrum of PP before and after adsorption exhibits a large absorption peak at 3292 cm^{-1}, indicating the presence of OH groups resulting from vibrations of hemicellulose, cellulose, lignin, and adsorbed water [52]. The 2929 cm^{-1} peak corresponds to the stretching vibration of C–H in methyl groups. The stretching of C=O group of ketones and aldehydes is represented by the peak at 1720 cm^{-1} [53]. The peak at 1602 cm^{-1} is related to CH_2 stretching in the aromatic ring of hemicellulose. The phenolic, ether, ester, and carboxylic groups in lignin, cellulose, and hemicellulose components are responsible for the C–O stretching vibration at 1016 cm^{-1} [54,55]. Weak peaks at 1322 and 1439 cm^{-1} can be associated to δCH_3 bending and δCH_2 scissoring, respectively, in hemicelluloses (H_3C–(C=O)–O–) and lignin (H_3C–O–Ar) [56]. Additionally, the peak at 1634 cm^{-1} can be assigned to the aromatic ring, and the band at 1335 cm^{-1} represents the aromatic–N bond. However, the PP–SO spectrum shows important changes. A new peak appeared at 1216 cm^{-1} and could be assigned to the C–N stretching vibration in the amine group of SO [57], whereas the peak at 1417 cm^{-1} disappeared and the peak at 1720 cm^{-1} became more intense. These peaks are assigned to lignin, cellulose, and hemicellulose compounds, suggesting that these groups are mainly responsible for the adsorption of SO molecules on the PP surface, as confirmed by similar results obtained by Mekhamer et al. [28] and Oyekanmi et al. [58].

The XRD pattern in Figure 2b shows a spectrum typical of the amorphous zone of the cellulose material. It has primary and secondary peaks at 2θ of

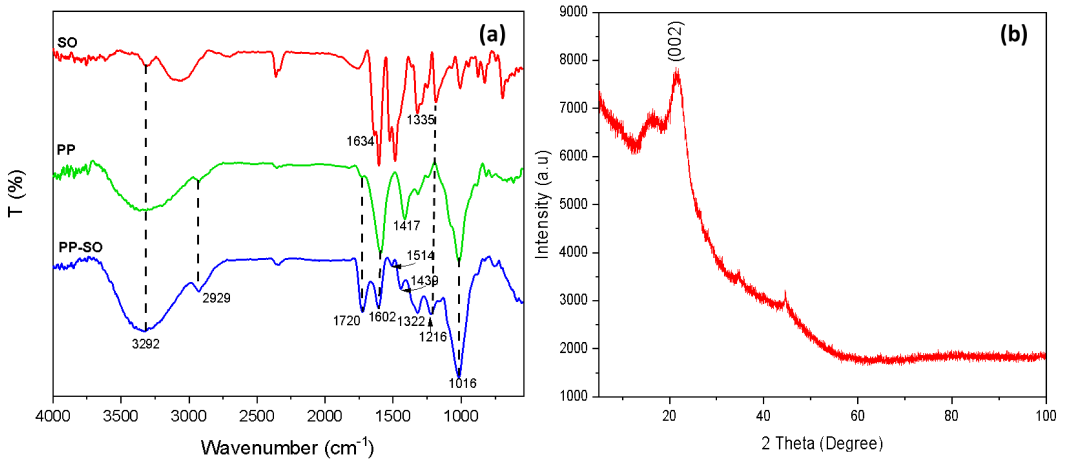

Figure 2. (a) FTIR spectrum of the SO dye, PP before adsorption and PP after adsorption of the dye; (b) XRD.

22 and 16, respectively, corresponding to the (002) plane. The primary peak indicates the presence of highly organized crystalline cellulose, whereas the secondary peak corresponds to a less organized polysaccharide structure. Based on X-ray line broadening, the Debye–Scherer formula ($D = K\lambda/\beta\cos\theta$) was used to get the PP size. The formula takes into account the average crystalline size (D), the X-ray wavelength used (λ), the angular width of the line at half maximum intensity (β), and the Bragg angle (θ) [59]. The estimated average size of the PP for the (002) reflection is 7.83 nm. These findings are consistent with those reported by other researchers like for instance Habibi et al. [60] who observed comparable crystalline sizes in cellulose derived from diverse sources, ranging from 5 to 8 nm, confirming the consistency of crystalline structures in natural cellulose materials [60].

The TGA profile of PP exhibits the characteristic behavior of cellulosic material (Figure 3). It was intended to be a lignocellulosic biomass consisting of cellulose, hemicellulose, and lignin [61]. The initial phase is ascribed to the evaporation of water. The subsequent degradation phases might be elucidated by the decomposition of organic material [62]. The final step pertains to carbonization, meaning the completion of organic material decomposition.

The electrical charge on the surface is mainly dependent on the point of zero charge (pH_{pzc}). As seen in Figure 4, the pH_{pzc} was determined by the intersection point of the pH_{final} versus $pH_{initial}$ curve with the bisector, which at 3.58 is not far from the value of 4.6 reported by Ben-Ali et al. [63], while a different pH_{pzc} value of 6.53 was obtained for Turkish pomegranate peel [64]. Consequently, the surface of PP had a positive charge when the solution pH was less than 3.58 and a negative charge when the pH of the solution was greater than 3.58. At lower pH values, the OH, COOH, and NH_2 groups became protonated whereas at higher pH values, they became deprotonated. This resulted in the negative charge of PP at pH > pH_{pzc}, which increased the electrostatic attraction with the SO molecules [65,66].

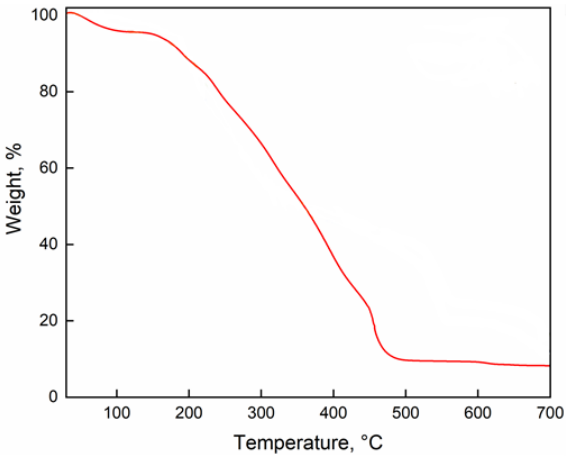

Figure 3. TGA analysis of PP.

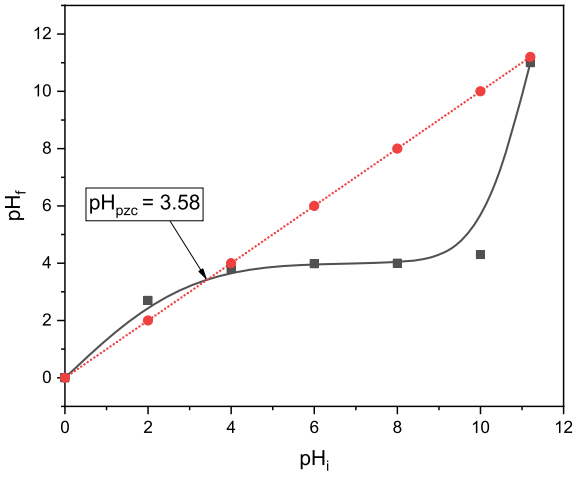

Figure 4. pH$_{pzc}$ of PP.

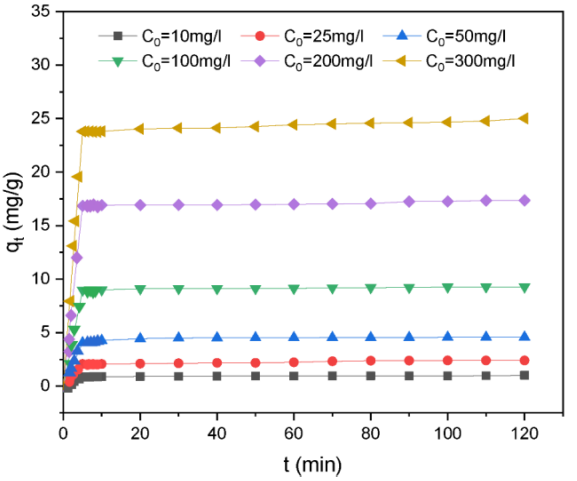

Figure 5. Effect of initial SO concentration and contact time on adsorption onto PP. Conditions: pH$_{natural}$ = 5.85, room temperature = 20 ± 2 °C, adsorbent dosage = 10 g/L.

The pH of the adsorbent was found to be 4.52. This pH value gave an idea about the acidic nature of the adsorbent. Moisture contents, ash contents, and bulk density were 9%, 11.98%, and 0.47 g/cm^3, respectively.

The Boehm titration of the surface functions, as shown in Table 1, proves that the concentration of the acidic functions is more important on the surface of the PP adsorbent (51.5 mmol/g), in agreement with the obtained adsorbent value (pH = 4.52).

The surface area was determined using the iodine number. The particle size was 0.315 mm, and the iodine number was 589 mg/g. The iodine molecule is relatively small, with an area of 0.4 nm^2, and it could enter the smaller micropores [67,68]. Consequently, the obtained value showed that PP had the highest adsorption capacities for iodine molecules and that the pores were primarily micropores (diameter < 2 nm). Furthermore, the specific surface area was calculated using the iodine number as follows [69,70]:

$$S = \frac{IN \times N \times A}{M_w} \tag{32}$$

where IN is the number of iodine molecules attached, N is the Avogadro constant (6.02×10^{23} mol^{-1}), A the size of the iodine surface area (0.2096×10^{-18} m^2), and M_w the molar mass of iodine (126.92 g/mol). Consequently, the specific surface area obtained was 585.56 m^2/g. The surface area and microporosity of active carbons were typically approximated using the iodine number with a high precision [70–72].

The results of the physical and chemical characterization of PP from this study are summarized in Table 1.

3.2. *Effect of physicochemical parameters on SO adsorption*

3.2.1. *Effect of initial dye concentration and contact time*

Figure 5 shows how the initial SO concentration (10–300 mg/L) affected SO adsorption. During the first five minutes, the amount of adsorbed SO increased quickly. After that, it increased more slowly over the next five to thirty minutes until saturation was reached. When SO concentration was increased from 10 to 300 mg/L, the equilibrium adsorption rose from 0.99 to 25.01 mg/g. The results show that, when the initial concentration was increased, a more significant mass transfer driving force led to higher SO adsorption because the initial concentration overcame all mass transfer resistances between the aqueous and solid phases [73]. To confirm that complete equilibrium had been reached, the experimental data were measured after 120 min.

Table 1. Physical and chemical properties of PP

Parameters	Experimental values
pH_{pzc}	3.58
pH	4.52
Bulk density (g/cm^3)	0.47
Moisture content (%)	9
Ash contents (%)	11.98
Textural properties	
Methylene blue number (mg/g)	24.9
Iodine number (mg/g)	589
Specific surface area (m^2/g)	585.56
Surface functional groups (mmol/g)	
Carboxylic function	7.57
Carbonyl function	16.53
Phenol function	27.4
Total acidic functions	51.5
Total basic functions	45

3.2.2. *Effect of adsorbent dosage*

Adsorbent dosage is an important parameter that needs to be carefully controlled during wastewater treatment. The effect of the PP adsorbent dose on the removal of SO (Figure 6) was studied by varying the adsorbent dosage (1–40 g/L); the initial concentration of SO was 50 mg/L in natural pH and room temperature. The SO removal efficiency per gram of PP increased with the adsorbent dosage, reaching a plateau of approximately 88%. Because of the increased surface area caused by the adsorbent dose, more active sites were created for SO adsorption, increasing the removal efficiency. A plateau was observed beyond 10 g/L of PP, indicating that the equilibrium between SO molecules in a bulk aqueous solution and the SO adsorbed on the PP surface was established at this dose with an initial SO concentration of 50 mg/L. However, the amount of SO adsorbed per gram of PP decreased with the increase in adsorbent dosage; this is probably because a stronger interaction between the PP particles caused the conglomeration of exchanger particles. As a result, the active sites overlapped, which prevented the dosage from significantly increasing the effective surface area [74]. From Figure 6, the adsorption process was insufficient to completely remove the SO dye. Additional treatments, such as advanced oxidation processes (AOPs), photocatalysis, electrochemical techniques, microbial or enzymatic biodegradation, and membrane filtration, such as reverse osmosis, were then recommended. The exploration of a combination of these methods might enhance dye removal efficiency.

3.2.3. *Effect of initial pH on adsorption*

The initial pH is a crucial factor affecting the process and the adsorption capacity. The ionic species of the adsorbed molecule and the surface charge of the adsorbent are both influenced by pH. SO adsorption was investigated in the pH range 2–12. From Figure 7, the results indicate that for pH = 2, the only value lower than that of the pH_{pzc}, the adsorption capacity and the removal efficiency are equal to 4.65 mg/g and 89.63%, respectively. For an increased pH of 4, close to the pH_{pzc} value of 3.58, the corresponding adsorption capacity and removal efficiency reach their highest values at 5.03 mg/g and 96.93%, respectively. Generally, for pH values below pH_{pzc}, electrostatic repulsion happens between the positively charged dye molecules and the positively charged adsorbent surface. Furthermore, lower SO adsorption at acidic

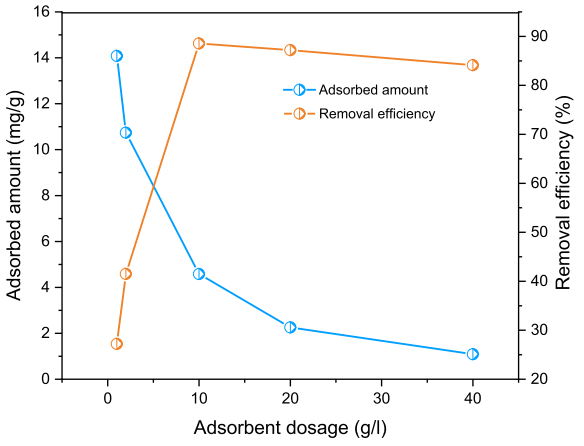

Figure 6. Effect of adsorbent dosage on SO adsorption by PP. Conditions: C_0 = 50 mg/L, $pH_{natural}$ = 5.85, room temperature = 20 ± 2 °C.

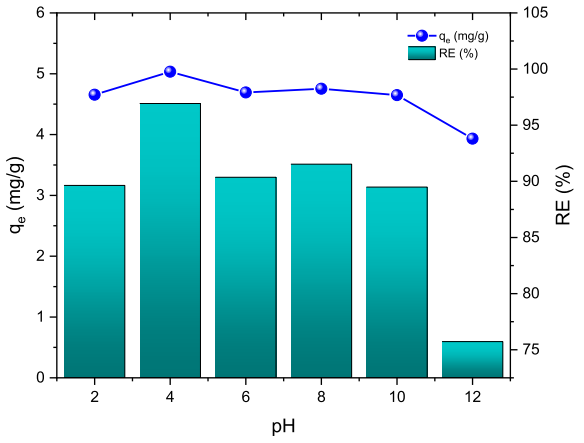

Figure 7. Effect of initial pH on SO adsorption capacity (q_e) and removal efficiency (RE) by PP. Conditions: C_0 = 50 mg/L, temperature = 20 ± 2 °C, adsorbent dosage = 10 g/L.

pH is caused by excess H^+ ions competing with dye cations on the active sites. At pH values greater than pH_{pzc}, the electrostatic force of attraction between the negatively charged surface of the PP and the positively charged dye cations increases [75]. The excess of OH^- ions interacts electrostatically with the dye cations to prevent them from adhering to the anionic sites of the adsorbent, which is why SO retention decreases at higher pH values.

3.3. *Kinetic study*

Determining the adsorbent adsorption efficiency requires an understanding of adsorption kinetics. This supports researchers in the design of the adsorption system and aids in the explanation of the adsorption mechanism [76]. Four models, pseudo-first-order (PFO), pseudo-second-order (PSO), Elovich, and intraparticle diffusion (IPD), were fitted to the experimental data to identify the step that controls the adsorption of SO onto the PP surface. The plots of the non-linear models are shown in Figure 8, whereas the linear fits of these models are shown in Figure 9. Table 2 summarizes the parameters and error values obtained through linear and non-linear regression of each model.

From Table 2, the error functions corresponding to the minimized deviations between the experimental equilibrium data and predicted kinetics suggest that PSO is the best fit followed by Elovich. By comparing the error functions of SSE and RMSE obtained by linear and non-linear regression methods, it can be observed that the error functions of the non-linear method are reduced except that of the Elovich model, where the error functions are not changed for the non-linear regression method; this could be explained by the great similitude between the linear and non-linear equation forms for this model.

The numerous paths to predict the applicable kinetic adsorption models to the experimental data indicate that PSO is better at modeling the adsorption process. On the other hand, comparing the statistical parameters (R^2, SSE, and RMSE) and $q_{e,exp}$ versus $q_{e,cal}$ for non-linear and linear PSO for the three different SO concentrations (50, 200, and 300 mg/L) onto PP adsorbent show that linear PSO is more appropriate with high R^2, small values of SSE and RMSE, and relatively similar values for $q_{e,cal}$ and $q_{e,exp}$ (Table 2). For the Elovich model, it can be observed that the error functions are not changed for linear and non-linear methods. The lower R^2 values of the IPD kinetic model indicate that this model is not applicable for predicting the SO adsorption kinetics/dynamic behavior. This means that the adsorption rate was not limited by mass transfer of SO from the solution to the external surface of PP.

The results show that the determination coefficients of R^2 values are higher for PSO models than for PFO. The higher R^2 values indicate that PSO more

Table 2. Kinetic parameters and error functions of the linear and non-linear models for adsorption at three initial concentrations of SO onto PP

Kinetic model	Coefficients	50 mg/L		100 mg/L		300 mg/L	
		Non-linear	Linear	Non-linear	Linear	Non-linear	Linear
Pseudo-first-order	$q_{e,\mathrm{exp}}$ (mg·g^{-1})	4.5828	4.5828	9.2691	9.2691	25.018	25.018
	$q_{e,\mathrm{cal}}$ (mg·g^{-1})	4.3159	0.5698	0.5305	9.0399	23.673	2.2304
	k_1 (min^{-1})	1.8897	0.0350	0.0339	3.5394	2.6739	0.0179
	R^2	0.9172	0.9342	0.8746	0.9037	0.1527	0.9416
	SSE	2.8795	1.2530	4.3047	0.4904	12.658	0.5219
	RMSE	0.3999	0.2503	0.4890	0.1566	0.8163	0.1702
Pseudo-second-order	$q_{e,\mathrm{cal}}$ (mg·g^{-1})	4.4470	4.5943	9.1045	9.2652	24.095	24.801
	k_2 (g·mg^{-1}·min^{-1})	0.7866	0.2911	1	0.3031	0.3119	0.0642
	R^2	0.6429	0.9999	0.0028	0.9999	0.5654	0.9998
	SSE	0.5652	0.0674	0.5518	0.0171	6.4932	0.0089
	RMSE	0.1724	0.0595	0.1704	0.0300	0.5845	0.0216
Elovich	$q_{e,\mathrm{cal}} = 1/\beta$ (mg·g^{-1})	0.1842	0.3684	0.1098	0.2197	0.5705	1.1411
	α (mg·g^{-1}·min^{-1})	1.2×10^{8}	9632.8	2.9×10^{33}	3.6×10^{16}	3.1×10^{16}	2.7×10^{8}
	β (g·mg^{-1})	5.4276	2.7138	9.1015	4.5508	1.7526	0.8763
	R^2	0.9383	0.9383	0.9544	0.9544	0.9509	0.9533
	SSE	0.0976	0.0976	0.0252	0.0252	0.6967	0.6967
	RMSE	0.0716	0.0716	0.0364	0.0364	0.1914	0.1914
Intraparticle diffusion	K_{i1} (mg·g^{-1}·min$^{-1/2}$)	0.0764	0.1703	0.2220	0.0586	0.2452	0.4667
	C_1 (mg·g^{-1})	3.8726	3.6272	7.4881	8.7396	22.340	21.7904
	R_1^2	0.8494	0.8785	0.1617	0.9197	0.2211	0.8299
	SSE	0.2383	0.0361	65.668	0.0027	427.34	0.4025
	RMSE	0.1119	0.0634	1.8120	0.0173	4.6224	0.2114
	K_{i2} (mg·g^{-1}·min$^{-1/2}$)	-	0.0094	-	0.0145	-	0.0591
	C_2 (mg·g^{-1})	-	4.4514	-	9.0164	-	23.715
	R_2^2	-	0.8626	-	0.9507	-	0.8108
	SSE	-	1.1×10^{-4}	-	3.1×10^{-5}	-	0.0010
	RMSE	-	0.0054	-	0.0039	-	0.0322
	K_{i3} (mg·g^{-1}·min$^{-1/2}$)	-	0.0241	-	0.031	-	0.1594
	C_3 (mg·g^{-1})	-	4.3181	-	8.9240	-	23.050
	R_3^2	-	0.9736	-	0.9780	-	0.9511
	SSE	-	1.8×10^{-5}	-	1.3×10^{-5}	-	0.0041
	RMSE	-	0.0030	-	0.0036	-	0.0371
	K_{i4} (mg·g^{-1}·min$^{-1/2}$)	-	-	-	0.0083	-	0.7686
	C_4 (mg·g^{-1})	-	-	-	9.1781	-	16.597
	R_4^2	-	-	-	0.9989	-	1
	SSE	-	-	-	3.3×10^{-8}	-	-
	RSME	-	-	-	1.8×10^{-4}	-	-
	D_i (cm^2·s^{-1})	4.9×10^{-7}		2.4×10^{-7}		8.2×10^{-8}	

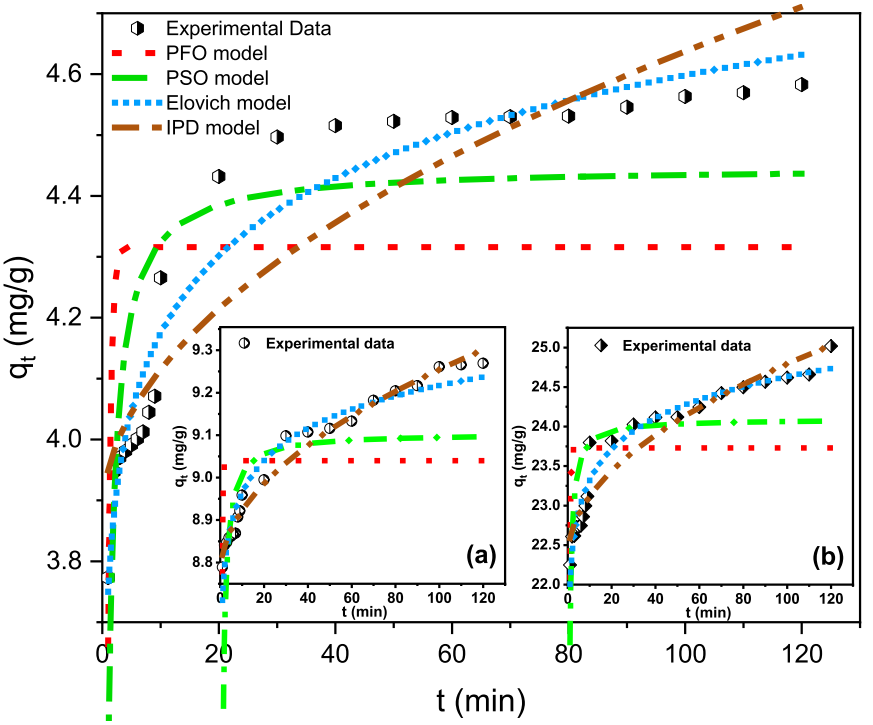

Figure 8. Non-linear kinetic models of SO adsorption by PP at different dye concentrations; inset (a) and (b) represent the non-linear kinetic models for C_0 = 100 mg/L and C_0 = 300 mg/L, respectively. Conditions: $pH_{natural}$ = 5.85, room temperature = 20 ± 2 °C, adsorbent dosage = 10 g/L.

closely modelled the adsorption process than PFO. When SO was adsorbed onto PP, R^2 values ranged from 0.9998 to 0.9999 for PSO models, more significant than the PFO model range of 0.9037 to 0.9416. Moreover, there is a similarity between the experimental adsorption capacities $q_{e,\mathrm{exp}}$ and the calculated adsorption capacities $q_{e,\mathrm{cal}}$ evaluated from the PSO model; this implies that the adsorption process is chemisorption, meaning that ion exchange between the adsorbent and the adsorbate is the rate-limiting step in the adsorption of SO onto PP.

Equation (15) was used to fit the Elovich model to the experimental data. The results are shown in Figure 9c and are plotted as q_t versus $\ln t$. Table 2 lists the values of α and β derived from the plots. According to the viability of the Elovich equation, the adsorption process is controlled by the chemisorption mechanism. Furthermore, a second-order model type was described by an Elovich model with the assumption that the solid surface was energetically heterogeneous. The Elovich model does not match the experimental data for SO adsorption by PP in view of the difference between $q_{e,\mathrm{exp}}$ and $q_{e,\mathrm{cal}}$ values.

The mechanism of dye diffusion could not be determined by using the PFO and PSO models only. This is because they incorporate every stage of the adsorption process, including intraparticle, external film, and adsorption diffusion. As a result, the IPD model was applied to provide the required information regarding the rate-limiting mechanisms [77]. The adsorption capacity was proportional to the square root of time. It indicates boundary layer resistance if the straight line does not cross the origin. The parameters are listed in Table 2, and q_t versus the square root of time $t^{0.5}$ is shown at various dye concentrations in Figure 9d. In the IPD plots, boundary-layer diffusion is theoretically represented by up to four linear regions. Following these regions, IPD occurred in macro, meso, and micropores. The system at equilibrium should then be represented by a horizontal line following these four regions [78]. For a dye concentration of 50 mg/L, the plots in Figure 9d display three regions, suggesting that boundary-layer

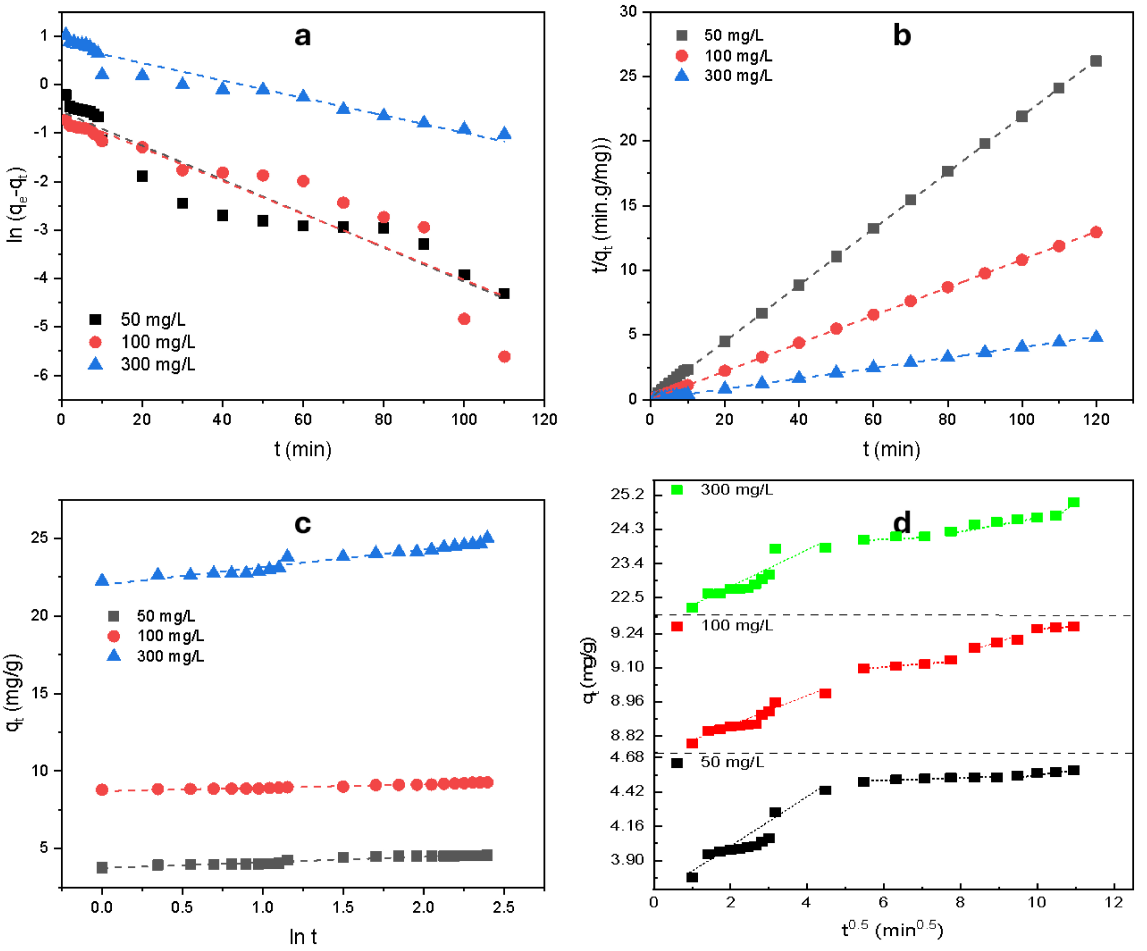

Figure 9. Kinetic models of SO adsorption by PP at different dye concentrations; (a) pseudo-first-order model, (b) pseudo-second-order model, (c) Elovich model and (d) Intraparticle diffusion model. Conditions: $pH_{natural}$ = 5.85, room temperature = 20 ± 2 °C, adsorbent dosage = 10 g/L.

diffusion was probably the rate-limiting step. Four observable regions exist for more concentrated solutions with C_0 > 50 mg/L. The fact that the intercept did not cross the origin ($C \neq 0$) suggests that other factors besides IPD also affected how quickly SO adsorbed onto PP. Similar findings with the use of pomegranate peels for removing dyes were reported by Ahmed et al. and Ververi et al. [79,80]. In Table 2, the pore diffusion coefficient D_i varies from 10^{-6} to 10^{-8} $cm^2 \cdot s^{-1}$, which indicates that film diffusion was the rate-limiting step. As a result, several steps were involved in the dye adsorption onto PP with other processes helping to regulate the adsorption rate [81].

Therefore, compared to the other models examined, the PSO kinetic model can better explain the adsorption of SO on PP, followed by the IPD model.

3.4. *Adsorption isotherm*

The adsorption isotherm is critical for understanding the reactive interactions between the solute and the adsorbent. It also aids in describing various parameters, such as the adsorbent surface area, the maximum capacity of adsorption, and the nature of the adsorbent, whether multilayer or monolayer. Adsorption isotherms were investigated using four models: the Langmuir isotherm, the Freundlich

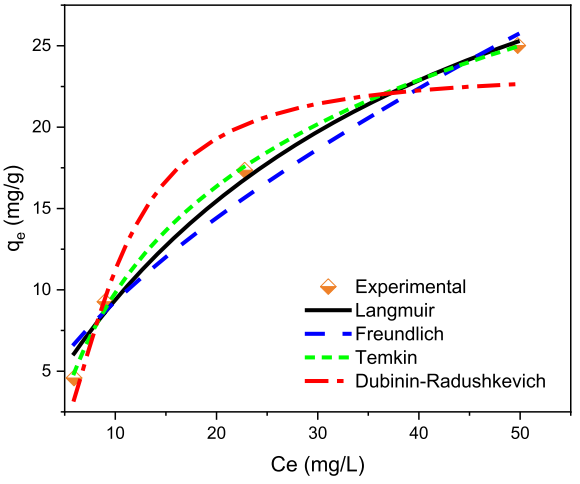

Figure 10. Fitting of the Langmuir, Freundlich, Temkin, and Dubinin–Radushkevich isotherm models to the experimental equilibrium data of SO adsorption by PP. Conditions: C_0 = 50–300 mg/L, $pH_{natural}$ = 5.85, room temperature = 21 ± 2 °C, adsorbent dosage = 10 g/L.

isotherm, the Temkin isotherm, and the Dubinin–Radushkevich (D–R) isotherm, as shown in Figure 10. Figure 8 shows the non-linear plots of the various isotherms. Table 3 lists the equilibrium constants and the corresponding fit of linear and non-linear isothermal constants, determination coefficients (R^2), and error functions for each model.

The Langmuir concept assumes that the adsorption occurs on the individual homogeneous monolayer of the adsorbent. Parameters for non-linear and linear isothermal models are summarized in Table 3. The q_m and b Langmuir constants were calculated for the non-linear model by fitting the q_e versus C_e plot curve and for the linear model by fitting $1/q_e$ versus $1/C_e$. The value of q_m was 44 and 152.67 for the non-linear and linear Langmuir models, respectively, while b was 0.027 for the non-linear model and 173.68 for the linear model. In comparison, the non-linear model R^2 (0.9874) was greater than the linear model R^2 (0.942). Based on the Langmuir model, the R_L value for the non-linear model is in the range of 0.1–0.42, implying that the SO adsorption process using PP was favorable ($0 < R_L < 1$), while $R_L > 1$ for the linear model indicates that the adsorption process was unfavorable [44]. As a consequence, the non-linear model of Langmuir would match the experimental adsorption data better than the linear model. According to the results obtained from the non-linear model of Langmuir, the adsorption process was carried out in a monolayer manner, demonstrating that SO had a comparatively high adsorption rate. The maximum adsorption amount of PP was confirmed by Langmuir (q_m = 44 mg/g). Additionally, because only one SO molecule was adsorbed by the active site on the PP surface [82], the affinity of SO for the adsorption sites on the surface was low (b = 0.0027), suggesting a weak interaction between adsorbate and adsorbent. Comparable results were found by Guzel et al. [64] for the removal of methylene blue using raw PP with a q_m value of 36.36 mg/g at 303 K. In another study, Ahmed et al. [79] found that the Freundlich model best fitted the experimental data for the removal of Remazol brilliant blue reactive dye onto PP activated carbon with a maximum adsorption capacity of 370.86 mg/g.

By comparing the error functions obtained by linear and non-linear regression methods for Freundlich, Temkin, and D–R models, it can be observed that the error functions of the non-linear method are reduced except that of the Temkin isotherm model, where the error functions are not changed for the non-linear regression method; this could be explained by the great similitude between the linear and non-linear forms for this model.

Two parameters were used to analyze the Freundlich model: the linearized form's adsorption intensity (n) and adsorption capacity (K_f). In this investigation, the K_f value was 1.45 L/g, indicating a high SO adsorption amount (Table 3). The high adsorption intensity of PP in this study (n = 1.32), which suggests a chemisorption process, shows that PP favorably adsorbed SO cations and formed noticeably stronger bonds with the PP adsorbent. As a result, multilayer adsorption on top of the already chemisorbed layer might be used to continue the adsorption of SO cations on PP. Moreover, the high R^2 value (0.9394) implies a role for multilayer adsorption in the mechanism's process.

The Temkin isotherm model confirmed the presence of heterogeneous sites with varying binding energies, which is consistent with the experimental findings. Based on the results in Table 2, the Temkin model was found to be appropriate for SO adsorption on PP, as evidenced by the highest R^2 value

Table 3. Isotherm parameters calculated from linear and non-linear models for SO adsorption onto PP

Isotherm model	Parameters	Linear	Non-linear
Langmuir	q_m (mg·g^{-1})	152.67	44.008
	b (L·mg^{-1})	173.68	0.0270
	R_L	1.15–1.91	0.1–0.42
	R^2	0.9420	0.9874
	SSE	0.0011	3.0486
	RMSE	0.0236	1.2346
Freundlich	n	1.3211	1.5756
	K_f ((mg·g^{-1})·(L·mg^{-1})1/n)	1.4516	2.1537
	R^2	0.9394	0.9671
	SSE	0.1009	8.0021
	RMSE	0.2246	2.0002
Temkin	a_T (L·g^{-1})	0.2828	0.2828
	B	9.4388	9.4388
	b_T (J·mol^{-1})	258.08	258.08
	R^2	0.9985	0.9985
	SSE	0.3539	0.3539
	RMSE	0.4206	0.4206
D–R	Q_m (mg·g^{-1})	3.0823	23.382
	K_d (mol^2·kJ^{-2})	1.1×10^{-7}	81.047
	E (kJ·mol^{-1})	2132	0.0785
	R^2	0.9670	0.9376
	SSE	0.054	15.202
	RMSE	0.1655	2.7570

(0.9985). These findings prove that chemisorption was involved in the SO adsorption process. The higher b value (258.08 J/mol) indicates a strong ion exchange mechanism and interaction between SO and the PP surface, which decreased the dye adsorption heat in the layer. In another study, a high value of b (139.52 KJ/mol) was found by Ismi et al. [83]; it demonstrated that the adsorption experiment followed a chemical process, indicating strong chemical bonds between adsorbate and adsorbent [83].

The D–R isotherm model determines whether the process of adsorption is physical (E < 8 kJ/mol) or chemical (E > 16 kJ/mol). The average adsorption energy (E, kJ/mol) is proportional to the energy required to transport dye molecules to the surface of the adsorbent [84]. The mean free energy (E) for PP in this investigation was greater than 16 kJ/mol (2132 kJ/mol), indicating that the SO adsorption process is chemical [49].

Since the R^2 values for the Temkin, Langmuir, Freundlich, and D–R adsorption isotherms are all greater than 0.93, it can be concluded that multilayer physisorption on top of the previously chemisorbed layer played a significant role in the multi-mechanistic SO adsorption by PP.

Table 4 displays a comparison of maximum adsorption capacity (q_m value) with other researchers who used PP as an adsorbent and the removal of SO with different adsorbents found in the literature. Compared to other adsorbents, PP has a comparable adsorption capacity for SO. Therefore, PP is suitable for SO elimination from aqueous solutions as it has a relatively high adsorption capacity.

Table 4. Comparison of Langmuir isotherm's maximum adsorption capacity q_m for adsorption of SO on various adsorbents and of other dyes on pomegranate peel

Adsorbent	Adsorbate	Conditions					q_m (mg/g)	Ref.
		pH	T (°C)	C_0 (mg/L)	Adsorbent dosage (g/L)	Contact time (min)		
Peanut husks	Safranin O	Natural	Room temperature	-	0.03	180	86.1	[85]
Soybean hulls	Safranin O	8	50	20–100	0.04	90	29.49	[86]
Mango seeds	Safranin O	10	-	50–300	1	400	43.47	[87]
Tea leaves	Safranin O	5	25	10–50	0.15	20	14.814	[88]
Thuja orientalis	Safranin O	7	10	5–25	0.125	60	0.17	[89]
PP	Malachite green	5	40	50	0.1	90	31.45	[29]
PP	Methylene blue	-	30	25–300	1	1440	250	[32]
PP	Sulfasalazine	-	25	50–200	0.5	120	64.04	[90]
PP	Ciprofloxacin hydrochloride	4–5	25	5000–10,000	0.01	120	999	[28]
PP	Safranin O	5.8	Room temperature	50–300	0.5	120	44	This work

3.5. *Thermodynamic properties*

A thermodynamic investigation was carried out at different temperatures (293 to 333 K) to examine the adsorption of SO by PP. The Van't Hoff equation was used to study the various thermodynamic parameters for the adsorption of SO onto PP, including the standard Gibbs free energy change ($\Delta G°$ kJ·mol^{-1}), standard change in entropy ($\Delta S°$ J·K^{-1}·mol^{-1}), and standard change in enthalpy ($\Delta H°$ kJ·mol^{-1}). The plot of ln K_d versus $1/T$ is shown in Figure 11, and Table 5 summarizes the thermodynamic parameters.

The negative $\Delta G°$ values indicate that SO adsorption onto PP is thermodynamically favored. In addition, even more negative values were found as the temperature increased gradually from 20 to 60 °C, indicating that the adsorption process became more favorable and most feasible at high temperatures. In addition, the negative values came from the increase in energy released when the dye interacted with the adsorbent surface. The fact that the $\Delta H°$ value of PP was positive (77.987 kJ·mol^{-1}) indicates that the SO adsorption process was endothermic [91]. The negative value of the entropy change ($\Delta S°$ = −0.271 kJ/mol) indicates a random decrease in adsorption occurring at the solid–liquid interface. Similar results were obtained by Penghi Li et al. and Ben Ali et al. [54,92]. Physisorption can be defined by $\Delta G°$ values over −20 kJ/mol, chemisorption from −80 kJ/mol to −400 kJ/mol. In this investigation, the values of Gibbs free energy varied from −1.416 kJ/mol to −12.25 kJ/mol. Consequently, the adsorption occurred as physisorption.

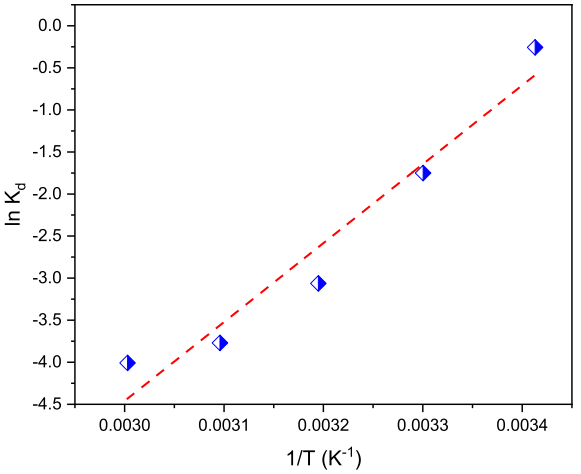

Figure 11. The plot of ln K_d versus $1/T$ for the adsorption of SO by PP, Conditions: C_0 = 50 mg/L, $pH_{natural}$ = 5.85, adsorbent dosage = 10 g/L.

Table 5. Thermodynamic parameters for SO adsorption by PP

Temperature (K)	$\Delta G°$ (kJ·mol^{-1})	$\Delta H°$ (kJ·mol^{-1})	$\Delta S°$ (kJ·mol^{-1}·K^{-1})
293	−1.416	77.987	−0.271
303	−4.126		
313	−6.836		
323	−9.546		
333	−12.25		

4. Conclusion

The recovery of agri-food waste and the effectiveness of pomegranate peel (PP) as adsorbent for removing the organic pollutant Safranin O (SO) in a synthetic medium has been highlighted in this study. Many methods were used to characterize its structure, such as pH_{pzc} analysis, XRD, FTIR, Boehm titration, and iodine number. Its ability to adsorb the SO dye was investigated at various pH values, temperatures, and initial dye concentrations. The adsorption process was rapid, achieving equilibrium after two hours of contact, with maximum dye uptake occurring within the initial 30 min. The adsorbent dose selected was 10 g/L. The dye removal percentage slightly decreased beyond 10 mg/L of adsorbent due to overcrowding of the sorbent. The PP adsorbent showed the highest SO removal efficiency, with a removal rate of up to 96.93%, under acidic conditions (pH = 4). The adsorption of SO was shown to be chemisorption when fitted to the pseudo-second-order kinetic model. The adsorption of SO onto PP was confirmed to occur through different stages by the multilinearity displayed by the intraparticle diffusion models. The fact that the intercept did not pass through the origin suggests other rate-determining steps besides intraparticle diffusion. The isotherms of SO adsorption onto PP followed the Temkin and Langmuir isotherm models. The obtained maximum monolayer adsorption capacity (q_m) was 44 mg/g in a 50–300 mg/L range. The values of $\Delta H°$ (77.987 kJ/mol) suggest that the adsorption process of SO was endothermic [92]. The negative values of $\Delta G°$ indicate that the adsorption of SO was favored. The adsorption mechanisms for SO onto PP were physisorption and chemisorption based on the obtained data. As a result, inexpensive PP appears as a promising adsorbent for the removal of cationic dyes from wastewater, including SO.

Declaration of interests

The authors do not work for, advise, own shares in, or receive funds from any organization that could benefit from this article, and have declared no affiliations other than their research organizations.

References

[1] W. J. Cosgrove and D. P. Loucks, "Water management: Current and future challenges and research directions", *Water Resour. Res.* **51** (2015), pp. 4823–4839.

[2] A. Ayat, S. Arris, A. Abbaz, M. Bencheikh-Lehocine and A. H. Meniai, "Application of response surface methodology for modeling and optimization of a bio coagulation process (sewage wastewater treatment plant)", *Environ. Manage.* **67** (2021), no. 3, pp. 489–497.

[3] D. Ghosh, S. Chaudhary, S. Sarkar and P. Singh, "Water pollution in rural areas: primary sources, associated health issues, and remedies", in *Water Resources Management for Rural Development*, Elsevier, 2024, pp. 15–28.

[4] V. Sivakumar and P. G. Rao, "Studies on the use of power ultrasound in leather dyeing", *Ultrason. Sonochem.* **10** (2005), no. 2, pp. 31–35.

[5] J. Sokolowska-Gajda, H. S. Freeman and A. Reife, "Synthetic dyes based on environmental considerations. Part 2: iron complexed formazan dyes", *Dyes Pigm.* **30** (1996), no. 1, pp. 1–20.

[6] K. Kusumlata, B. Ambade, S. Gautam and A. Kumar, "Sustainable solutions: reviewing the future of textile dye contaminant removal with emerging biological treatments", *Limnol. Rev.* **24** (2024), no. 2, pp. 126–149.

[7] A. Ayat, S. Arris, A. Abbaz and H. Aissaoui, "The removal of methylene blue and COD by coagulation using cactus", *Alg. J. Eng. Res.* **5** (2022), no. 2, pp. 1–6.

[8] E. A. Moawed and A. B. Abulkibash, "Selective separation of Light green and Safranin O from aqueous solution using Salvadora persica (Miswak) powder as a new biosorbent", *J. Saudi Chem. Soc.* **20** (2016), S178–S185.

[9] A. Asfaram, M. Ghaedi, A. Goudarzi and M. Rajabi, "Response surface methodology approach for optimization of simultaneous dye and metal ion ultrasound-assisted adsorption onto Mn doped Fe_3O_4-NPs loaded on AC: kinetic and isothermal studies", *Dalton Trans.* **44** (2015), no. 33, pp. 14707–14723.

[10] M. Fayazi, D. Afzali, M. A. Taher, A. Mostafavi and V. K. Gupta, "Removal of Safranin dye from aqueous solution using magnetic mesoporous clay: optimization study", *J. Mol. Liq.* **212** (2015), pp. 675–685.

[11] A. Flilissa, K. Laouameur, N. Hammoudi, et al., "Bentonite SDBS-loaded composite for methylene blue removal from wastewater: an experimental and theoretical investigation", *Environ. Res.* **241** (2024), article no. 117544.

[12] M. N. Chong, B. Jin, C. W. K. Chow and C. Saint, "Recent developments in photocatalytic water treatment technology: a review", *Water Res.* **44** (2010), no. 10, pp. 2997–3027.

[13] M. S. Khan, M. Khalid, M. S. Ahmad, M. Shahid and M. Ahmad, "Catalytic activity of Mn(III) and Co(III) complexes: evaluation of catechol oxidase enzymatic and photodegradation properties", *Res. Chem. Intermed.* **46** (2020), no. 6, pp. 2985–3006.

[14] I. Ali, "New generation adsorbents for water treatment", *Chem. Rev.* **112** (2012), no. 10, pp. 5073–5091.

[15] S. Wang and Y. Peng, "Natural zeolites as effective adsorbents in water and wastewater treatment", *Chem. Eng. J.* **156** (2010), no. 1, pp. 11–24.

[16] D. Azzouni, E. M. Saoudi Hassani, Z. Rais and M. Taleb, "An excellent alternative to industrial activated carbons for the purification of textile water elaborated from waste coffee grounds", *Int. J. Environ. Res.* **16** (2022), no. 5, article no. 89.

[17] F. Deniz and R. A. Kepekci, "Dye biosorption onto pistachio by-product: a green environmental engineering approach", *J. Mol. Liq.* **219** (2016), pp. 194–200.

[18] V. K. Gupta, P. J. M. Carrott, M. M. L. Ribeiro Carrott and V. S. Suhas, "Low-cost adsorbents: growing approach to wastewater treatmenta review", *Crit. Rev. Environ. Sci. Technol.* **39** (2009), no. 10, article no. 783842.

[19] S. Kainth, P. Sharma and O. P. Pandey, "Green sorbents from agricultural wastes: a review of sustainable adsorption materials", *Appl. Surf. Sci. Adv.* **19** (2024), article no. 100562.

[20] A. Sarker, R. Ahmmed, S. M. Ahsan, J. Rana, M. K. Ghosh and R. Nandi, "A comprehensive review of food waste valorization for the sustainable management of global food waste", *Sustain. Food Technol.* **2** (2024), no. 1, pp. 48–69.

[21] A. Silva, C. Delerue-Matos, S. A. Figueiredo and O. M. Freitas, "The use of algae and fungi for removal of pharmaceuticals by bioremediation and biosorption processes: a review", *Water* **11** (2019), no. 8, article no. 1555.

[22] S. Jmai, S. Guiza, S. Jellali, M. Bagane and M. Jeguirim, "Competitive bio-sorption of basic dyes onto petiole palm tree wastes in single and binary systems", *C. R. Chim.* **25** (2022), no. S2, pp. 27–41.

[23] S. Arris, I. Abbaz, M. Kassir, A. Abbaz, A. Ayat and M. Bencheikh Lehocine, "Optimization of phenol sorption in aqueous solution by date stone through response surface methodology", *Alger. J. Eng. Res.* **5** (2022), no. 2, pp. 28–34.

[24] G. T. Tee, X. Y. Gok and W. F. Yong, "Adsorption of pollutants in wastewater via biosorbents, nanoparticles and magnetic biosorbents: a review", *Environ. Res.* **212** (2022), article no. 113248.

[25] M. A. Ahmad, M. A. Eusoff, P. O. Oladoye, K. A. Adegoke and O. S. Bello, "Optimization and batch studies on adsorption of Methylene blue dye using pomegranate fruit peel based adsorbent", *Chem. Data Coll.* **32** (2021), article no. 100676.

[26] A. Ali, K. Egzar, N. Mustafa Kamal, N. abdulsaheb and M. Saleh Mashkour, "Removal of Amaranth Dye from aqueous solution using pomegranate peel", *Int. J. Basic Appl. Sci.* **13** (2013), no. 3, pp. 57–64.

[27] R. Giri, N. Kumari, M. Behera, et al., "Adsorption of hexavalent chromium from aqueous solution using pomegranate peel as low-cost biosorbent", *Environ. Sustain.* **4** (2021), no. 2, pp. 401–417.

[28] W. Mekhamer and S. Al-Tamimi, "Removal of ciprofloxacin from simulated wastewater by pomegranate peels", *Environ. Sci. Pollut. Res.* **26** (2019), no. 3, pp. 2297–2304.

[29] F. Gündüz and B. Bayrak, "Biosorption of malachite green from an aqueous solution using pomegranate peel: equilibrium modelling, kinetic and thermodynamic studies", *J. Mol. Liq.* **243** (2017), pp. 790–798.

[30] S. Ben-Ali, I. Jaouali, S. Souissi-Najar and A. Ouederni, "Characterization and adsorption capacity of raw pomegranate peel biosorbent for copper removal", *J. Clean. Prod.* **142** (2017), pp. 3809–3821.

[31] S. Talekar, A. F. Patti, R. Vijayraghavan and A. Arora, "Complete utilization of waste pomegranate peels to produce a hydrocolloid, punicalagin rich phenolics, and a hard carbon electrode", *ACS Sustain. Chem. Eng.* **6** (2018), no. 12, pp. 16363–16374.

[32] M. A. Ahmad, M. A. Eusoff, P. O. Oladoye, K. A. Adegoke and O. S. Bello, "Optimization and batch studies on adsorption of Methylene blue dye using pomegranate fruit peel based adsorbent", *Chem. Data Coll.* **32** (2021), article no. 100676.

[33] H. Thagira Banu, P. Karthikeyan and S. Meenakshi, "Lanthanum (III) encapsulated chitosan-montmorillonite composite for the adsorptive removal of phosphate ions from aqueous solution", *Int. J. Biol. Macromol.* **112** (2018), pp. 284–293.

[34] M. Farahani, S. R. S. Abdullah, S. Hosseini, S. Shojaeipour and M. Kashisaz, "Adsorption-based cationic dyes using the carbon active sugarcane bagasse", *Procedia Environ. Sci.* **10** (2011), pp. 203–208.

[35] M. A. Ahmad and N. K. Rahman, "Equilibrium, kinetics and thermodynamic of Remazol Brilliant Orange 3R dye adsorption on coffee husk-based activated carbon", *Chem. Eng. J.* **170** (2011), no. 1, pp. 154–161.

[36] E. CEFIC, *Test methods for activated carbon*, European Council Of Chemical Manufacturers Federation/European Chemical Industry Council: Brussels, 1986, pp. 9–43.

[37] M. A. Ahmad and N. K. Rahman, "Equilibrium, kinetics and thermodynamic of Remazol Brilliant Orange 3R dye adsorption on coffee husk-based activated carbon", *Chem. Eng. J.* **170** (2011), no. 1, pp. 154–161.

[38] S. K. Lagergren, "About the theory of so-called adsorption of soluble substances", *Kungl. Svenska Vetenskapsakad. Handl.* **24** (1898), pp. 1–39.

[39] Y.-S. Ho and G. McKay, "Pseudo-second order model for sorption processes", *Process Biochem.* **34** (1999), no. 5, pp. 451–465.

[40] W. J. Weber and J. C. Morris, "Kinetics of adsorption on carbon from solution", *J. Sanit. Eng. Div.* **89** (1963), no. 2, pp. 31–59.

[41] A. E. Ofomaja, E. B. Naidoo and A. Pholosi, "Intraparticle diffusion of Cr (VI) through biomass and magnetite coated biomass: a comparative kinetic and diffusion study", *S. Afr. J. Chem. Eng.* **32** (2020), no. 1, pp. 39–55.

[42] M. Shaban, M. E. M. Hassouna, F. M. Nasief and M. R. AbuKhadra, "Adsorption properties of kaolinite-based nanocomposites for Fe and Mn pollutants from aqueous solutions and raw ground water: kinetics and equilibrium studies", *Environ. Sci. Pollut. Res.* **24** (2017), no. 29, pp. 22954–22966.

[43] I. Langmuir, "The adsorption of gases on plane surfaces of glass, mica and platinum", *J. Am. Chem. Soc.* **40** (1918), no. 9, pp. 1361–1403.

[44] M. R. Abukhadra, A. Adlii and B. M. Bakry, "Green fabrication of bentonite/chitosan@ cobalt oxide composite (BE/CH@ Co) of enhanced adsorption and advanced oxidation removal of Congo red dye and Cr (VI) from water", *Int. J. Biol. Macromol.* **126** (2019), pp. 402–413.

[45] H. M. F. Freundlich, "Over the adsorption in solution", *J. Phys. Chem.* **57** (1906), no. 385471, pp. 1100–1107.

[46] N. F. El-Harby, S. M. A. Ibrahim and N. A. Mohamed, "Adsorption of Congo red dye onto antimicrobial terephthaloyl thiourea cross-linked chitosan hydrogels", *Water Sci. Technol.* **76** (2017), no. 10, pp. 2719–2732.

[47] M. I. Temkin, "Kinetics of ammonia synthesis on promoted iron catalysts", *Acta Physiochim. URSS* **12** (1940), pp. 327–356.

[48] M. M. Dubinin, "The equation of the characteristic curve of activated charcoal", *Dokl. Akad. Nauk. SSSR* **55** (1947), pp. 327–329.

[49] H. A. El-Araby, A. M. M. A. Ibrahim, A. H. Mangood and A.-H. Adel, "Sesame husk as adsorbent for copper (II) ions removal from aqueous solution", *J. Geosci. Environ. Protect.* **5** (2017), no. 07, article no. 109.

[50] A. Abbaz, S. Arris, G. Viscusi, A. Ayat, H. Aissaoui and Y. Boumezough, "Adsorption of Safranin O Dye by alginate/pomegranate peels beads: kinetic, isotherm and thermodynamic studies", *Gels* **9** (2023), no. 11, article no. 916.

[51] M. Wakkel, B. Khiari and F. Zagrouba, "Comprehensive study of simultaneous adsorption of basic red 2 and basic violet 3 by an agro-industrial waste: dynamics, kinetics and modeling", *C. R. Chim.* **23** (2020), no. 11–12, pp. 671–687.

[52] A. Hashem, C. O. Aniagor, M. F. Nasr and A. Abou-Okeil, "Efficacy of treated sodium alginate and activated carbon fibre for Pb (II) adsorption", *Int. J. Biol. Macromol.* **176** (2021), pp. 201–216.

[53] S. Saadat, Z. Emam-Djomeh and G. Askari, "Antibacterial and antioxidant gelatin nanofiber scaffold containing ethanol extract of pomegranate peel: design, characterization and in vitro assay", *Food Bioprocess Technol.* **14** (2021), pp. 935–944.

[54] S. Ben-Ali, I. Jaouali, S. Souissi-Najar and A. Ouederni, "Characterization and adsorption capacity of raw pomegranate peel biosorbent for copper removal", *J. Clean. Prod.* **142** (2017), pp. 3809–3821.

[55] H. Belmabrouk, M. Selmi, T. Alshahrani, et al., "Cationic dye removal using Pergularia tomentosa L. fruit: kinetics and isotherm characteristics using classical and advanced models", *C. R. Chim.* **25** (2022), no. S2, pp. 61–79.

[56] A. Boukir, S. Fellak and P. Doumenq, "Structural characterization of Argania spinosa Moroccan wooden artifacts during natural degradation progress using infrared spectroscopy (ATR-FTIR) and X-Ray diffraction (XRD)", *Heliyon* **5** (2019), no. 9, article no. e02477.

[57] N. C. Ozdemir, M. Saleh, Z. Bilici, H. Arslan and N. Dizge, "Preparation of leonardite powder-embedded calcium alginate beads and adsorption of Safranin-O dye", *Water Pract. Technol.* **18** (2023), no. 7, pp. 1711–1726.

[58] A. A. Oyekanmi, A. Ahmad, S. H. M. Setapar, et al., "Sustainable *Durio zibethinus*-derived biosorbents for congo red removal from aqueous solution: Statistical optimization, isotherms and mechanism studies", *Sustainability (Switzerland)* **13** (2021), no. 23, article no. 13264.

[59] S. I. Siddiqui and S. A. Chaudhry, "Nigella sativa plant based nanocomposite-$MnFe_2O_4$/BC: an antibacterial material for water purification", *J. Clean. Prod.* **200** (2018), pp. 996–1008.

[60] Y. Habibi, L. A. Lucia and O. J. Rojas, "Cellulose nanocrystals: chemistry, self-assembly, and applications", *Chem. Rev.* **110** (2010), no. 6, pp. 3479–3500.

[61] İ. Demiral, A. Eryazıcı and S. Şensöz, "Bio-oil production from pyrolysis of corncob (*Zea mays* L.)", *Biomass Bioenergy* **36** (2012), pp. 43–49.

[62] S. Ben-Ali, I. Jaouali, S. Souissi-Najar and A. Ouederni, "Characterization and adsorption capacity of raw pomegranate peel biosorbent for copper removal", *J. Clean. Prod.* **142** (2017), pp. 3809–3821.

[63] S. Ben-Ali, "Application of raw and modified pomegranate peel for wastewater treatment: a literature overview and analysis", *Int. J. Chem. Eng.* **2021** (2021), no. 1, article no. 8840907.

[64] F. Güzel, Ö. Aksoy and G. Akkaya, "Application of pomegranate (Punica granatum) pulp as a new biosorbent for the removal of a model basic dye (methylene blue)", *World Appl. Sci. J.* **20** (2012), no. 7, pp. 965–975.

[65] E. Kavci, "Malachite green adsorption onto modified pine cone: Isotherms, kinetics and thermodynamics mechanism", *Chem. Eng. Commun.* **208** (2021), no. 3, pp. 318–327.

[66] M. Z. Momèilović, A. E. Onjia, M. M. Purenović, A. R. Zarubica and M. S. Randelović, "Removal of a cationic dye from water by activated pinecones", *J. Serb. Chem. Soc.* **77** (2012), no. 6, pp. 761–774.

[67] A. Baçaoui, A. Yacoubi, A. Dahbi, et al., "Optimization of conditions for the preparation of activated carbons from olive-waste cakes", *Carbon NY* **39** (2001), no. 3, pp. 425–432.

[68] M. N. Alaya, M. A. Hourieh, A. M. Youssef and F. El-Sejariah, "Adsorption properties of activated carbons prepared from Olive Stones by chemical and physical activation", *Adsorp. Sci. Technol.* **18** (2000), no. 1, pp. 27–42.

[69] C.-H. Wu, "Studies of the equilibrium and thermodynamics of the adsorption of Cu^{2+} onto as-produced and modified carbon nanotubes", *J. Colloid Interf. Sci.* **311** (2007), no. 2, pp. 338–346.

[70] A. Mianowski, M. Owczarek and A. Marecka, "Surface area of activated carbon determined by the iodine adsorption number", *Energy Sources, Part A* **29** (2007), no. 9, pp. 839–850.

[71] C. Saka, "BET, TG–DTG, FT-IR, SEM, iodine number analysis and preparation of activated carbon from acorn shell by chemical activation with ZnCl2", *J. Anal. Appl. Pyrolysis* **95** (2012), pp. 21–24.

[72] C. A. Nunes and M. C. Guerreiro, "Estimation of surface area and pore volume of activated carbons by methylene blue and iodine numbers", *Quim. Nova* **34** (2011), no. 3, pp. 472–476.

[73] K. Mahmoudi, N. Hamdi, M. Ben Ali, S. Jellali and E. Srasra, "Enhanced adsorptive removal of cationic and anionic dyes from aqueous solutions by olive stone activated carbon", *C. R. Chim.* **23** (2020), no. 11–12, pp. 689–704.

[74] S. Jellali, M. A. Wahab, M. Anane, K. Riahi and N. Jedidi, "Biosorption characteristics of ammonium from aqueous solutions onto Posidonia oceanica (L.) fibers", *Desalination* **270** (2011), no. 1, pp. 40–49.

[75] G. Crini, H. N. Peindy, F. Gimbert and C. Robert, "Removal of C.I. Basic Green 4 (Malachite Green) from aqueous solutions by adsorption using cyclodextrin-based adsorbent: Kinetic and equilibrium studies", *Sep. Purif. Technol.* **53** (2007), no. 1, pp. 97–110.

[76] W. A. Khanday, M. Asif and B. H. Hameed, "Cross-linked beads of activated oil palm ash zeolite/chitosan composite as a bio-adsorbent for the removal of methylene blue and acid blue 29 dyes", *Int. J. Biol. Macromol.* **95** (2017), pp. 895–902.

[77] S. Banerjee, R. K. Gautam, A. Jaiswal, M. Chandra Chattopadhyaya and Y. Chandra Sharma, "Rapid scavenging of methylene blue dye from a liquid phase by adsorption on alumina nanoparticles", *RSC Adv.* **5** (2015), no. 19, pp. 14425–14440.

[78] C. C. O. Alves, A. S. Franca and L. S. Oliveira, "Evaluation of an adsorbent based on agricultural waste (corn cobs) for removal of tyrosine and phenylalanine from aqueous solutions", *Biomed. Res. Int.* **2013** (2013), article no. 978256.

[79] M. A. Ahmad, N. A. A. Puad and O. S. Bello, "Kinetic, equilibrium and thermodynamic studies of synthetic dye removal using pomegranate peel activated carbon prepared by microwave-induced KOH activation", *Water Resour. Ind.* **6** (2014), pp. 18–35.

[80] M. Ververi and A. M. Goula, "Pomegranate peel and orange juice by-product as new biosorbents of phenolic compounds from olive mill wastewaters", *Chem. Eng. Process.—Process Intensif.* **138** (2019), pp. 86–96.

[81] H. Zeng, Y. Zeng, H. Xu, S. Sun, J. Zhang and D. Li, "Sb(III) Removal by Granular Adsorbent synthesized with iron-containing water treatment residuals and chitosan", *Polymers (Basel)* **16** (2024), no. 22, article no. 3214.

[82] N. F. Al-Harby, E. F. Albahly and N. A. Mohamed, "Kinetics, isotherm and thermodynamic studies for efficient adsorption of congo red dye from aqueous solution onto novel cyanoguanidine-modified chitosan adsorbent", *Polymers (Basel)* **13** (2021), no. 24, article no. 4446.

[83] I. Ismi, E. Rifi and A. Lebkiri, "Application of Kinetic and isotherm models to the Sorption of Copper (II) on to superabsorbent polymer in powder form", *Mor. J. Chem.* **2** (2014), no. 4, pp. 403–414.

[84] M. Mourabet, H. El Boujaady, A. El Rhilassi, et al., "Defluoridation of water using Brushite: Equilibrium, kinetic and thermodynamic studies", *Desalination* **278** (2011), no. 1, pp. 1–9.

[85] I. Safarik and M. Safarikova, "Magnetic fluid modified peanut husks as an adsorbent for organic dyes removal", *Phys. Procedia* **9** (2010), pp. 274–278.

[86] V. Chandane and V. K. Singh, "Adsorption of safranin dye from aqueous solutions using a low-cost agro-waste material soybean hull", *Desal. Water Treat.* **57** (2016), no. 9, pp. 4122–4134.

[87] M. R. M. Mohamad Rasool Malekbala, S. M. S. Salman Masoudi Soltani, S. K. Y. Sara Kazemi Yazdi and S. H. Soraya Hosseini, "Equilibrium and kinetic studies of safranine adsorption on alkali-treated mango seed integuments", *Int. J. Chem. Eng. Appl.* **3** (2012), no. 3, pp. 160–166.

[88] S. S. Nehaba, R. H. Abdullah, A. M. Oda, A. R. Omran and A. S. Mottaleb, "Evaluation of the efficiency of tea waste powder to remove the Safranin O dye compared to the activated carbon as adsorbent", *Orient. J. Chem.* **35** (2019), no. 3, pp. 1201–1207.

[89] D. E. Al-Mammar, "Decolorization of the aqueous Safranin O dye solution using Thuja orientalis as biosorbent", *Iraqi J. Sci.* **55** (2014), no. 3A, pp. 886–898.

[90] M. C. Bouallegue, B. Trifi, I. Marzouk Trifi, O. Zahraa and A. Alatrache, "Removal of an emerging pharmaceutical pollutant, sulfasalazine, by adsorption onto pomegranate peels", *Chem. Eng. Commun.* **209** (2022), no. 7, pp. 957–966.

[91] M. Jain, A. Mudhoo and V. K. Garg, "Swiss blue dye sequestration by adsorption using Acacia nilotica sawdust", *Int. J. Environ. Technol. Manage.* **14** (2011), no. 1–4, pp. 220–237.

[92] P. Li, C. Yang, Y. Wang, W. Su, Y. Wei and W. Wu, "Adsorption studies on the removal of anionic and cationic dyes from aqueous solutions using discarded masks and lignin", *Molecules* **28** (2023), no. 8, article no. 3349.